Effect of Guest–Host Hydrogen Bonding on the Structures and Properties of Clathrate Hydrates

Saman Alavi,* Konstantin Udachin, and John A. Ripmeester*[a]

Abstract: To provide improved understanding of guest–host interactions in clathrate hydrates, we present some correlations between guest chemical structures and observations on the corresponding hydrate properties. From these correlations it is clear that directional interactions such as hydrogen bonding between guest and host are likely, although these have been ignored to greater or lesser degrees because there has been no direct structural evidence for such interactions. For the first time, single-crystal X-ray crystallography has been used to detect guest–host hydrogen bonding in structure II (sII) and structure H (sH) clathrate hydrates. The clathrates studied are the *tert*-butylamine (*t*BA) sII clathrate with H_2S/Xe help gases and the pi-

nacolone + H_2S binary sH clathrate. X-ray structural analysis shows that the *t*BA nitrogen atom lies at a distance of 2.64 Å from the closest clathrate hydrate water oxygen atom, whereas the pinacolone oxygen atom is determined to lie at a distance of 2.96 Å from the closest water oxygen atom. These distances are compatible with guest–water hydrogen bonding. Results of molecular dynamics simulations on these systems are consistent with the X-ray crystallographic observations. The *t*BA guest shows long-lived guest–host hydrogen bonding with the nitrogen atom

tethered to a water HO group that rotates towards the cage center to face the guest nitrogen atom. Pinacolone forms thermally activated guest–host hydrogen bonds with the lattice water molecules; these have been studied for temperatures in the range of 100–250 K. Guest–host hydrogen bonding leads to the formation of Bjerrum L-defects in the clathrate water lattice between two adjacent water molecules, and these are implicated in the stabilities of the hydrate lattices, the water dynamics, and the dielectric properties. The reported stable hydrogen-bonded guest–host structures also tend to blur the longstanding distinction between true clathrates and semiclathrates.

Introduction

Clathrate hydrates,[1,2] or gas hydrates, are a topic of great interest today, primarily because of the promise of vast quantities of natural gas trapped in gas hydrates, both under permafrost[3] and offshore on continental margins.[3] An older interest is that of a hydrate hazard for the oil and gas industries, in which hydrates are capable of blocking pipelines for oil and gas transport.[4] This has generated a branch of petroleum engineering known as flow assurance, which is

concerned with the development of methods to prevent pipeline blockage.

These are the oldest[5] and arguably the best understood class of supramolecular materials, but some problems remain in, for instance, prediction of hydrate formation, understanding of guest distributions over hydrate cages, and other physicochemical properties. The main criterion for hydrate formation is that water must be in contact with suitable molecular guests under appropriate conditions (p, T, concentration). The guests must fill the hydrate cages to a certain minimum extent in the three common structures—cubic structure I (sI), cubic structure II (sII), and hexagonal structure H (sH) hydrates[1]—as required by free energy considerations.[6] This poses a question as to which molecules are in fact appropriate for hydrate formation. Of the known hydrate-forming guest molecules, of which there are around 150,[7] methane is by far the most common guest, because it occurs in the ubiquitous natural gas hydrates. On the other hand, methanol, also of an appropriate size, is

[a] Dr. S. Alavi, Dr. K. Udachin, Prof. J. A. Ripmeester
Steacie Institute for Molecular Sciences
National Research Council of Canada
100 Sussex Dr., Ottawa, ON, K1A 0R6 (Canada)
E-mail: saman.alavi@nrc-cnrc.gc.ca
         john.ripmeester@nrc-cnrc.gc.ca

known only as an inhibitor of hydrate formation.[8] Very recently, several papers have dealt with the "surprising" observation that ethanol, better known as a hydrate inhibitor, as well as well as other alcohols, was also able to function as a hydrate guest.[9] Clearly, between these two extremes in behavior—hydrate guests versus hydrate inhibitors—we should expect a range of hydrate-forming propensities for small, water-soluble molecules and different physiochemical properties of the hydrates formed. Such a concept counters a generally held opinion that the guest molecule does not affect the properties of the hydrate "very much".[10] This opinion is also reflected in the idea that to predict clathrate hydrate properties only non-specific van der Waals interactions between guest and host need to be taken into account,[6] although such a model would actually predict that methanol should form a hydrate. This assumption, really a first-order approximation, is still the underpinning of most of the hydrate prediction software that use hybrid molecular/thermodynamic approaches in which empirical interaction potentials are obtained by their adjustment to fit various macroscopic properties.[11] What is lost in this approach is the connection between the macroscopic (thermodynamic) view of hydrate formation and a molecular understanding of guest–host interactions.

So, which of the properties of hydrates are known to show trends that depend on the chemical structure of the guest molecule? First of all, if we examine a number of hydrates with guest molecules of similar size and shape, it becomes quite clear that there are trends in the stabilities of the hydrates as judged by the decomposition conditions. Table 1 shows that hydrates with oxygen-containing guests tend to decompose at lower temperatures than either the related hydrocarbons or the sulfur analogue guests.[7] Another, and related, trend is that of the temperature-dependent dielectric properties.[8] At 240 K, the dielectric relaxation times are some three orders of magnitude shorter for hydrates with oxygen-containing guests than for those with other guests. This was attributed to faster water molecule reorientation in hydrates with oxygen-containing guests, also giving activation energies for this process that are smaller by nearly a factor of two. In turn, the smaller activation energies were attributed to transient hydrogen-bond formation between the guest oxygen and host water molecules, thus in-

jecting Bjerrum-like defects into the hydrate lattice because of misoriented water molecules. These dielectric observations have been well corroborated by NMR measurements, giving a consistent view of water dynamics.[12] Within the subgroup of hydrates of oxygen-containing guests, there is a second correlation: that of dielectric permittivity with the dipole moment of the guest molecule.[12]
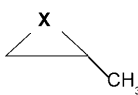
Recently, molecular dynamics (MD) simulations of hydrates have indicated support for hydrogen bonding between oxygen-containing guests and host water.[13] Both transient and persistent hydrogen bonds were observed. The details of guest–host hydrogen bonding on the MD timescale appear to depend on the presence of oxygen in the guest, the dipole moment, and the location of the guest in the cage as dictated by guest size and shape. In addition, the number of guest–host hydrogen bonds and the corresponding defects in the water lattice may increase or decrease with temperature, depending on whether the hydrogen bonded guest–host structure is more stable than the host–host hydrogen bond at low temperatures. However, no evidence of hydrogen bonding was observed on examination of X-ray structural data for hydrates (tetrahydrofuran, dimethyl ether, acetone) for which dielectric, NMR, and MD simulations showed evidence of hydrogen bonding. What must be taken into account, however, is that the X-ray technique produces an average "snapshot" of the entire structure. To observe the hydrogen bonds, there must at any time be a significant fraction of water–guest hydrogen bonds relative to the total number of water–water hydrogen bonds in the system.

Evidence from a diverse set of observations, including dielectric relaxation measurements, NMR relaxation times, and MD simulations, has thus implicated both guest–host hydrogen bonds and guest dipole moments in shaping some hydrate properties. The timescales of these modes of observation are very different: stability is a static thermodynamic property, dielectric and NMR relaxation have microsecond or slower timescales, and MD simulations are carried out on timescales of tens of picoseconds to nanoseconds. At this stage, some clarifying observations would be very helpful for placing the importance of specific guest–host interactions on a firmer footing. Conclusive evidence of the role of guest–host hydrogen bonding could be expected from the propensities of small molecules to act both as hydrate formers and as hydrate inhibitors. Quantification of this complex concept would thus offer a way of advancing hydrate prediction that takes details at the molecular level into account.

Another reason for interest in the guest–host interactions is that many water-soluble clathrate-forming guests with potential to hydrogen bond with the clathrate hydrate lat-

Table 1. Hydrate decomposition conditions for various guests.

Guest molecule	X	Structure	T [°C] (p[a] [atm])	Guest molecule	X	Structure	T [°C] (p[a] [atm])
⬜—X	CH₂	II	> 14	△—X	CH₂	I	16.2 (5.59)
	O	II	−9.2		O	I	11.1
	S	II	11.7		S	I	12.2
CH₃XCH₃	CH₂	II	5.7 (5.45)	CH₃X	CH₃	I	14.7 (33.5)
	O	II	−20.7		OH	I	no hydrate
	S	II	2.6		SH	I	12.0 (1.25)
CH₃CH₂X	CH₃	II	5.7 (5.45)	△—X (CH₃)	CH₂	II	5
	OH	II	−73.5		O	II	−3.5
	SH	II	3.4		S	II	2.6

[a] If a single figure is given, it is the melting point at ambient pressure or in a sealed tube. If two figures are given, these are the T, P values at the upper quadruple point in the phase diagram.

tice (such as tetrahydrofuran) act as "promoters" for hydrogen or methane storage.[14] These promoters lead to the formation of binary clathrates with hydrogen at much lower pressures than are required for the formation of the pure hydrogen clathrate. It is really not known how the promoter effect can be predicted.

Here we combine both direct X-ray structural data and MD simulation to validate the case for guest–host hydrogen bonding and discuss some of its effects. The systems studied are the pinacolone (*tert*-butyl methyl ketone) + H_2S binary sH clathrate hydrate and the *tert*-butylamine (*t*BA) + H_2S/ Xe sII clathrate hydrate.

Results and Discussion

Pinacolone + H_2S sH clathrate: The X-ray structure of pinacolone in the large sH cage, viewed looking parallel to the C6 axis (polar axis) of the cage at 100 K, is shown in Figure 1. The long axis of the molecule is oriented in the polar direction of the cage. The carbonyl oxygen of pinaco-
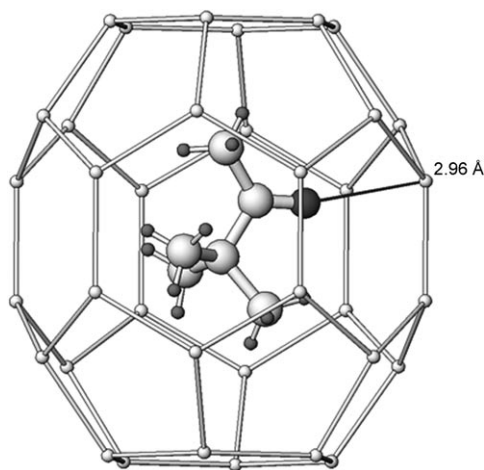

Figure 1. Experimentally determined X-ray structure for the pinacolone molecule in the sH large cage at 100 K. The full structure of the clathrate hydrate phase, including the H_2S guests in the small and medium sH cages, can be seen in the CIF files given in the Supporting Information.

lone is positioned at a distance of 2.96 Å from a water molecule in the equatorial plane of the large sH cage. Although the water hydrogen atom is not visible in this structure, the pinacolone-O···H−O−H distance is consistent with hydrogen bonding between the pinacolone molecule and the cage water. The oxygen atom of the hydrogen-bonded water molecule is not appreciably pulled out of the "ideal" position in the cage towards the pinacolone guest.

Simulations of the pinacolone + H_2S sH clathrate were performed for temperatures in the 100–250 K range. The position of a sample pinacolone molecule in a large cage from the MD simulation is shown in Figure 2. At 250 K the carbonyl oxygen interacts with "equatorial" water molecules of
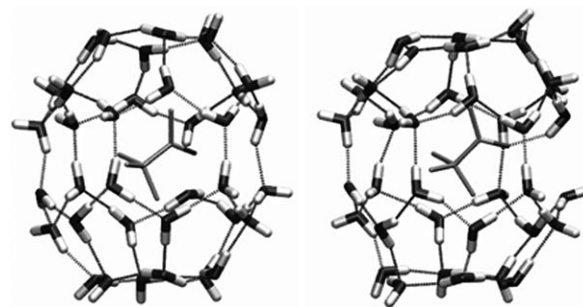

Figure 2. Snapshots of a large sH clathrate cage with a pinacolone guest molecule at 250 K. The guest–host hydrogen bond is show in the right-hand panel. The hydrogen bond is weak and does not lead to motion of the water oxygen atom out of its lattice site and distortion of the cage structure.

the large sH cages and forms transient hydrogen bonds as shown in the right-hand figure. In order for this to occur, a H−OH···OH_2 hydrogen bond in the lattice breaks and the −OH group rotates towards the hydrogen bond acceptor atom on the guest molecule. The guest–host bonding can be quantified by calculating the radial distribution functions (RDFs) for the pinacolone carbonyl oxygen (OS) with water oxygen (OW) and hydrogen (HW) atoms at 100 and 250 K, as shown in Figure 3. The OS–OW RDFs at both
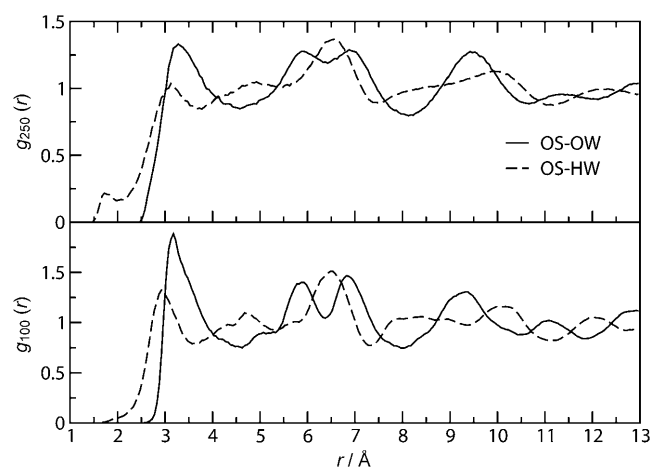

Figure 3. The RDFs for the oxygen atom (OS) of pinacolone with the lattice water oxygen atoms (OW) and hydrogen atoms (HW) at two temperatures. At 250 K a small peak at ~1.7 Å is observed in the OS–HW RDF. This short distance represented by this peak implies the formation of a guest–water hydrogen bond. The OS–OW RDF does not change significantly with temperature.

temperatures have peaks in the 3–3.5 Å range, consistently with the X-ray structure for this clathrate hydrate shown in Figure 1. At 250 K a small peak corresponding to the short distance of ~1.7 Å is observed in the OS–HW RDF, which implies the rotation of a water molecule so as to have the H−O bond face the pinacolone carbonyl oxygen. This structural feature is not pronounced at 100 K and these hydrogen

bonds are formed less frequently at this temperature. The guest–host hydrogen bonds are transient and do not greatly distort the clathrate cage structure (see below).

The criterion for the formation of a guest–host bond was whether the distance between the guest oxygen atom (OS) and a cage water hydrogen atom (HW) is less than 2.1 Å. We determined the probability of guest–host bond formation for ten pinacolone guest molecules in our simulation at times in the trajectory from

$$P(\text{guest} - \text{hostbonding}) = \frac{t(r \leq 2.1)}{t_{total}} \qquad (1)$$

where $t(r \leq 2.1)$ is the total time in the trajectory when the guest–host OS–HW distance is less than 2.1 Å and t_{total} is the total simulation trajectory time. The probabilities of guest–host bonding at four temperatures in the 100–250 K range are shown in Figure 4. The slope of the van't Hoff plot de-

Figure 5. The average lifetime of a pinacolone–water hydrogen bond at temperatures between 100–250 K. The times shown are in units of 0.25 ps.
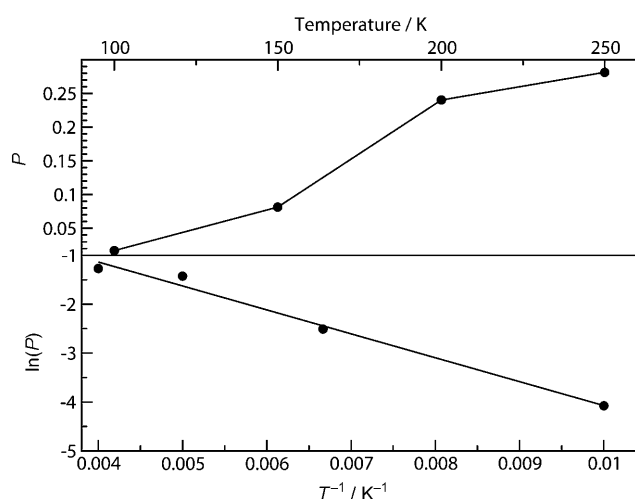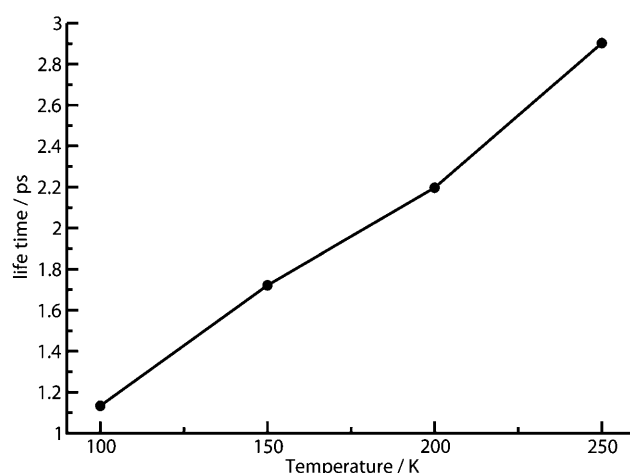

Figure 4. The probability of guest–host bond formation at different temperatures (top panel) and the van't Hoff plot for the change in probability of pinacolone–water bond formation at different temperatures (bottom panel). Good linearity is obtained in the van't Hoff plot.

rived from these probabilities allows us to determine the reaction enthalpy for guest–host hydrogen-bond formation as +4.1 kJ mol^{-1}. This result shows that the pinacolone–water hydrogen-bond formation is an endothermic process. The strengths of the hydrogen bonds between clathrate water lattice molecules are greater than that of the pinacolone–water hydrogen bond and thermal vibrations in the lattice are required to provide the activation energy required to break lattice bonds.

Average lifetimes for the guest–host hydrogen bonds can be determined by determining the number of continuous snapshots over which the pinacolone guest is hydrogen-bonded to the lattice water molecules. The average lifetimes for the hydrogen bonds at four temperatures are shown in Figure 5. The times shown are in units of 0.25 ps.
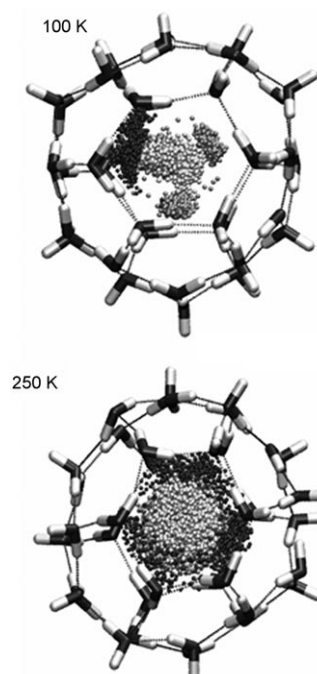

Figure 6. Overlapping orientations of the pinacolone molecule in a large sH cage at 100 and 250 K. At 100 K the rotation of the molecule in the equatorial plane is hindered in the timeframe of the simulation (250 ps). The black guest atoms represent oxygen.

The pinacolone guests undergo rotation in the equatorial planes of the large sH cages. Snapshots of the motion of a pinacolone guest over an observation window of 250 ps at 100 and at 250 K are shown in Figure 6. At low temperature (100 K) the pinacolone guest mostly associates with a potential energy well of a single equatorial hexagonal face and only undergoes hindered rotation within a limited range of azimuthal angles in the cages. As can be seen in Figure 4, the probability of pinacolone–water hydrogen bonding is small at 100 K. At 250 K, the pinacolone molecules have

more kinetic energy, but a greater probability of hydrogen-bond formation with the cage water molecules. As can be seen in Figure 5, the lifetimes of these hydrogen bonds are relatively short and the pinacolone guests dissociate from and reattach with waters of the hexagonal faces in the equatorial plane. As a result of the sizes of the pinacolone guests and the strong associations with cage water molecules, the lateral rotation of these guests in the large cages is still not free at high temperatures.

To quantify the rotation of the pinacolone guests, we define the orientational autocorrelation function (OACF) with reference to a unit vector $\mu(t)$ in the direction of the pinacolone C=O bond at each time t

$$OACF(t) = \langle \mu(t) \cdot \mu(0) \rangle = \langle \cos \theta(t) \rangle \qquad (2)$$

where the brackets represent an ensemble average over pinacolone guests. The OACF(t) = $\langle \cos \theta(t) \rangle$ gives a measure of the average change in orientation of the pinacolone molecules with time. The OACFs for pinacolone at different temperatures are plotted in Figure 7 and can be fitted to double exponential decay functions:

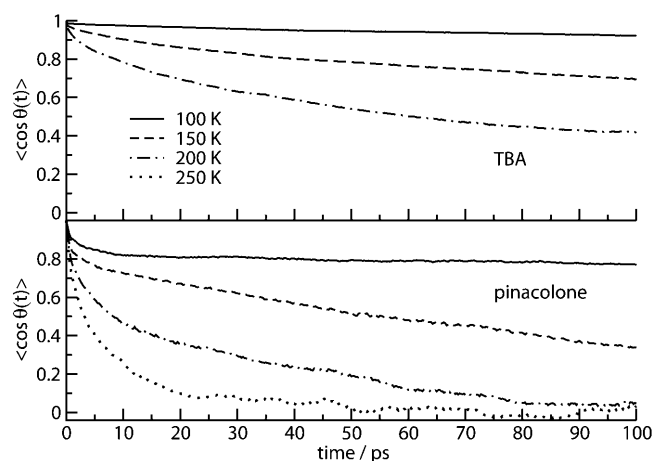$$OACF(t) = A e^{-t/\tau_1} + (1-A) e^{-t/\tau_2} \qquad (3)$$

Figure 7. The orientational autocorrelation function for the unit vector in the direction of the C=O bond in pinacolone at temperatures in the 100–250 K range and in the tBA molecule between 100 and 200 K.

The double exponential fit function allows for two distinct relaxation timescales—τ_1 and τ_2—to account for the decay of the OACF. The short time scale τ_2 represents the effect of high-frequency motions on the relaxation of the OACF, whereas the longer timescale τ_1 describes the decay of the OACF due to the rotation of the guest in the cage. The A parameter describes the relative contributions of the short- and long-timescale mechanisms to the decay of the OACF. The fit parameters A, τ_1, and τ_2 for pinacolone at different temperatures are given in Table 2. The two time constants τ_1

Table 2. Fit parameters for the orientational autocorrelation function of pinacolone + H$_2$S sH and the tBA + H$_2$S,Xe sII clathrate hydrate.

Molecule	Temperature	A	τ_1 [ps]	τ_2 [ps]
pinacolone	100	0.822	1567.7	2.00
	150	0.794	120.4	0.89
	200	0.622	38.5	1.78
	250	0.459	15.7	2.06
tBA	100	0.974	1776.2	4.0
	150	0.889	402.7	8.2
	200	0.765	150.3	7.3

and τ_2 measure the long-timescale (low frequency) rotations of the pinacolone guests in the water cage and the short-timescale vibrations of the pinacolone molecules in the local potential minimum (see Figure 6a), respectively. The τ_1 constant (which varies between 10^1 and 10^3 ps) decreases drastically with temperature. The τ_2 constant varies between 1 and 2 ps and remains relatively constant with temperature.

At higher temperatures, the kinetic energies of the pinacolone molecules increase and they can overcome the van der Waals barrier to rotation in the large sH cages within shorter times. This is reflected in the smaller value of τ_1 at higher temperature (see Table 2). On the other hand, as can be seen in Figures 4 and 5, the probability and lifetime of hydrogen-bond formation between pinacolone and the cage water molecules increases at higher temperatures. These factors tend to limit the range of angular motion of the pinacolone guests. Hydrogen bonding of pinacolone to cage water will result in a high frequency vibrational motion of the guest, characterized by the time constant τ_2. We see that at higher temperatures the A factor in Equation (3) increases as these high-frequency vibrations become more important in the angular dynamics of the guest. A combination of these conflicting factors leads to the decay of the OACF observed in Figure 7.

Another interesting aspect of the parameters shown in Table 2 is the change in the A factor with temperature. The decrease in the A factor at high temperatures shows that a simple unimolecular description of the pinacolone rotation is not sufficient to describe the rotational dynamics of the guest. Properties that depend on the rotational dynamics of the pinacolone guests, such as dielectric relation or NMR relaxation constants, will thus have complex temperature dependence.

***tert*-Butylamine + (H$_2$S, Xe) sII clathrate**: Pure tBA forms a structure VI clathrate hydrate upon compression with water.[25–27] In the presence of helper gases (a mixture of H$_2$S and Xe in the present case), tBA forms a sII clathrate hydrate.[27–29] The single-crystal X-ray structure of the binary tBA + H$_2$S/Xe sII hydrate gives the placement of the tBA molecule in the large sII cage as shown in Figure 8. The experimentally measured N–OW distance is determined as 2.64 Å. The experimentally determined structure shows that the water molecule hydrogen-bonded to the amine nitrogen has been displaced by about 1 Å towards the center of the
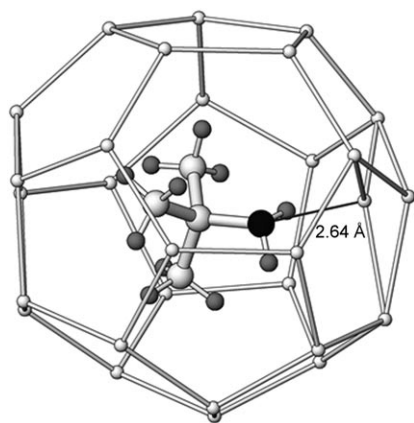
Figure 8. The position of *t*BA in the sII large cage determined by single-crystal X-ray crystal structure analysis. The NH–OW distance is determined to be 2.64 Å. The full structure of the clathrate hydrate phase, including the H_2S, Xe guests in the small sII cages, can be seen in the CIF files given in the Supporting Information.

cage from the ideal cage site. Dos et al.[30] have recently performed ab initio calculations to determine the gas-phase N···O distance in CH_3NH_2···HOH to be 2.855 Å. The confinement of the bulky *t*BA molecule in the relatively small size of the sII cages can perhaps explain the shorter hydrogen bond length in the clathrate. The powder pattern for the sII binary $tBuNH_2/H_2S$,Xe hydrate, as well as for a sII hydrate without H bonds, are given in the Supporting Information. We note that there are rather small differences in a number of reflection intensities in the usual analytical range of reflections used for phase identification, so routine PXRD is not likely to be able to distinguish the two forms of sII hydrate.

The configuration of a *t*BA molecule in the sII large cages as determined from molecular dynamics simulations is shown in Figure 9. At 90 K, the guest–host hydrogen bonds
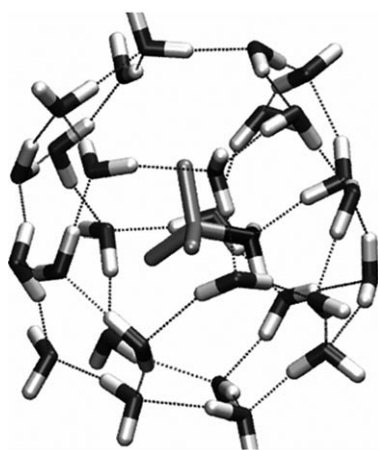

Figure 9. A snapshot of a large sII clathrate cage with a *tert*-butylamine guest molecule at 250 K. The guest–host hydrogen bond is formed between the amine nitrogen and a water oxygen atom. This hydrogen-bonded water is pulled out of its lattice site towards the center of the cage.

between the amine nitrogen and water H atoms are long-lived and tether the guest to a specific site in the cage. The guest–water hydrogen bond is the result of the rotation of a cage water molecule in such a way that one H−O bond in the clathrate hydrate water lattice faces the N atom hydrogen bond acceptor of the guest. This leads to the formation of a Bjerumm L-defect[30] in the clathrate hydrate water lattice. The *t*BA molecules occasionally detach from their water partners and undergo partial rotation in the cage before re-bonding to other water molecules. Consistent with the X-ray structure, the water molecule hydrogen-bonded to the amine nitrogen is pulled substantially inward towards the center of the clathrate cage.

The RDFs for the *t*BA nitrogen atom (NH) with the cage water oxygen (OW) and hydrogen (HW) atoms at 250 K are shown in Figure 10. A distinct peak in the NH–HW RDF at
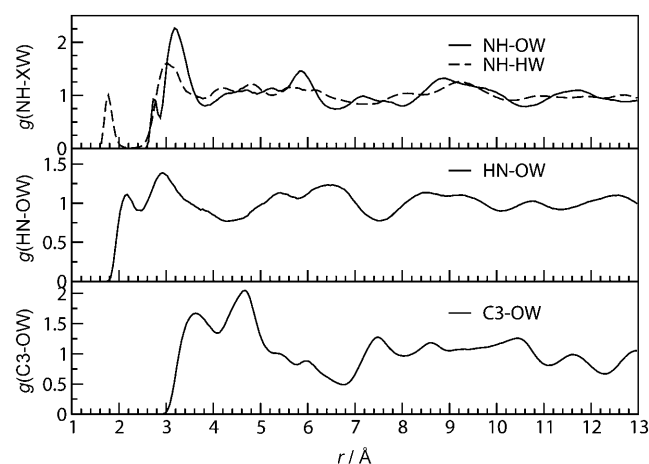

Figure 10. Top panel: the amine nitrogen (NH) RDFs with the water oxygen (OW) and hydrogen (HW) of the clathrate hydrate at 100 K. The strong NH–HW peak indicates strong hydrogen bonding between the guest and cage waters. Middle panel: the amine hydrogen (HN)–OW RDF. Bottom panel: the RDF of the C3 (methyl) carbon atoms in *t*BA with the OW atoms for reference.

t ~1.7 Å shows strong hydrogen bonding between these atoms. Moreover, there is a shoulder on the NH–OW RDF at about 2.6 Å, which shows that the hydrogen-bonded water molecule is pulled inwards from its ideal lattice position in the sII large cage. The location of the peak in the RDF for the NH–OW pair from the MD simulation is in excellent agreement with the experimentally determined value of 2.64 Å for the separation of these two atom types. This indicates that a strong hydrogen bond is formed between the *t*BA and the water cage molecules. The amine hydrogen atom (HN)–OW RDF is also shown in Figure 10 and shows a broad shoulder near 2.2 Å, which indicates the presence of hydrogen-bond interactions between the amine hydrogen atoms and the clathrate water molecules. There are no particular short-range correlations between the *t*BA carbon atoms and the cage oxygen atoms.

In the 100–200 K temperature range studied, the tBA–water bonds in the sII binary hydrate are long-lived and the probability of guest–host bond formation as defined in Equation (1) is greater than 95%. The strong guest–host bonding tethers the guest inside the cage and causes a slow decay of the orientational autocorrelation function. The orientational autocorrelation functions for tBA at three temperatures are shown in Figure 7. These OACFs are fit to the double exponential decay function [Eq. (3)] and the fit parameters are given in Table 2.

The decays in the OACF for tBA in the smaller sII cages are slower than those of pinacolone in the larger sH cages. The smaller τ_2 constant for tBA varies between 4–8 ps, whereas the large τ_1 constant decreases from 1800 to 150 ps as the temperature increases. Because of the strong hydrogen bonding between tBA and water the decay of the OACF is dominated by the τ_1 exponent in the range of temperatures studied.

The OACF decay parameters for tBA are comparable to those of tetrahydropyran (THP) in the sII clathrate large cages.[13] The THP guest forms similar strong guest–host bonds with the sII hydrate large-cage water molecules. Simulations of the tBA hydrate at 250 K and ambient pressure show that the hydrate decomposes under these conditions.

We note that tBA has a special place among clathrate-hydrate-forming guests. By itself, tBA forms a hydrate known as structure VI, a true clathrate without apparent hydrogen bonds between guest and host, at least from the structural work. This is different from other alkylamines, which form semiclathrates with unique structures in which guests form parts of the host lattices. However, with a second, small-cage guest present, tBA forms a sII hydrate with reasonably strong hydrogen bonding between guest and host, so there appear to be relatively subtle differences in the guest–host interactions for the two structures.

Conclusions

Hydrogen bonding of guest molecules with the cage water molecules in the pinacolone and $tert$-butylamine hydrates has been observed directly by single-crystal X-ray structure analysis. These hydrogen bonds lead to the formation of long-lived Bjerrum L-defects[31] in the water lattices of these hydrates. The guest–host associations affect the guest and host dynamics. The stronger basicity of the tBA amine group gives it stronger hydrogen bonds with the water molecules of the clathrate hydrate framework. For this molecule, the guest–framework water hydrogen bonds form at low temperatures. The weaker basicity of the pinacolone carbonyl oxygen makes the guest–host hydrogen bonds weaker than the water–water hydrogen bonds of the clathrate framework. For this guest, thermal excitation of the framework at higher temperatures is needed to weaken the water–water bonds to form pinacolone–water hydrogen bonds. These factors lead to the different types of hydrogen bonding behavior at different temperature for these two guest molecules.

We recently studied different classes of oxygen-containing guests in sII and sH clathrate hydrates with molecular dynamics simulations and NMR relaxation time studies. We observed that some oxygen- and nitrogen-containing guest molecules form hydrogen bonds with the water molecules of the clathrate framework. The hydrogen-bond formation for the different guest molecules follows two distinct types of behavior. For guests with relatively weak guest–water hydrogen bonds, such as pinacolone, the hydrogen-bond formation is enhanced at higher temperatures. For guests with relatively strong guest–water hydrogen bonds, such as tBA, hydrogen-bond formation is stronger at lower temperatures.

Semi-clathrate hydrates are clathrate hydrates of guest molecules with large organic moieties and hydrogen-bonding functional groups, mainly alkylamines.[24] In known semiclathrates, the functional groups of the guests are directly incorporated into the water lattices and form a number of unique crystal structures. In the cases of guests such as tBA, tetrahydropyran, and $tert$-butyl methyl ether (TBME), the water lattices of the clathrate hydrates still have the classical sII or sH structures, but the guest molecules nevertheless form long-lasting hydrogen bonds with the lattice water molecules. This can affect guest and host dynamics and the relative clathrate stability. However, the work presented here does in fact blur some of the distinction between the "true" clathrates and semiclathrates.

Experimental Section

Synthesis, X-ray data collection, and structure solution: The samples were prepared by placing powdered ice and the liquid guest in Pyrex tubes, ice being in slight excess. Each Pyrex tube was connected to a vacuum line with a ground glass joint. After cooling of the end of the Pyrex tube that contained the powdered ice and liquid guest in liquid nitrogen, air was removed under dynamic vacuum and a measured volume of the gas (sufficient to fill all of the small cages in the hydrate structures) was condensed on top of the frozen mixture. The tube was then flame-sealed, the cold mixture meanwhile being kept in liquid nitrogen. After sealing, the sample was allowed to warm slowly to −20 °C in a freezer. Single crystals of sufficient quality for X-ray diffraction grew slowly during storage over several years.

Single-crystal X-ray diffraction data were measured with a Bruker Apex 2 Kappa diffractometer at 100 K, with use of graphite monochromatized Mo$_{K\alpha}$ radiation ($\lambda = 0.71073$ Å). The unit cell was determined from randomly selected reflections obtained with the aid of the Bruker Apex 2 automatic search, center, index, and least squares routines. Integration was carried out with the program SAINT, and an absorption correction was performed with SADABS.[15] The crystal structures were solved by direct methods and the structure was refined by full-matrix, least-squares routines with the SHELXTL program suite.[16] All atoms were refined anisotropically. Hydrogen atoms on guest molecules were placed in calculated positions and allowed to ride on the parent atoms. Further details of the X-ray structures are provided in the Supporting Information.

Computational Methods

Molecular dynamics methods: The initial coordinates of the water oxygen atoms in the sII and sH clathrates were taken from clathrate X-ray crystallography.[17,18] The O−H bond lengths in water are fixed at 1.0 Å as per the SPC/E water potential model[19] and the initial positions of the water hydrogen atoms about the oxygen atoms were chosen randomly to be consistent with the ice rules with simultaneous minimization of the total dipole moments of the unit cell. For the sII clathrate simulations, cubic cells consisting of $2 \times 2 \times 2$ replicas of the unit cell with 1088 water molecules were used. For sH clathrates, the hexagonal simulation cell was chosen as a $3 \times 3 \times 3$ replica of the unit cell with 918 water molecules. The center of mass of each guest molecule was initially placed in the center of the cage and the guest positions were equilibrated during the simulation. The large molecules were described with the AMBER force field[20] with CHELPG atomic point charges[21] and when available, custom designed force fields were used for the small helper guest molecules. Further description of the force fields are given in reference [13] and the Supporting Information.

Isotropic constant pressure/temperature NpT molecular dynamics simulations on periodic simulation cells were performed with the DL POLY software program version 2.16.[22] The pressure was regulated by use of the modified Nosé–Hoover barostat algorithm[23] with thermostat and barostat relaxation times of 0.2 and 1.0 ps, respectively. The equations of motion were integrated by use of the Verlet leapfrog algorithm with a time step of 1 fs. Long-range electrostatic interactions were calculated by the Ewald summation method[24] with a precision of 1×10^{-6} and all intermolecular interactions in the simulation box were calculated within a cutoff distance of $R_{cutoff} = 13.0$ Å. All simulations were performed for a total time of 250 ps, with the first 50 ps used for temperature scaled equilibration. Dynamics calculations at each temperature and pressure were performed by starting with the final NpT configurations of the previous stage. Constant energy/volume NVE simulations for the dynamics were performed for a total of 250 ps with an equilibration time of 50 ps. Structural and dynamics parameters were extracted from the run times. Temperatures in the range from 100 K to 250 K at ambient pressure were studied for each clathrate. Because the SPC/E water potential underestimates the melting point of the I_h ice phase,[19] temperatures may need to be scaled before making quantitative comparisons between simulation results and experimental values. Ambient pressure was used in all simulations.

To study the formation of guest–host hydrogen bonds, the 28 water molecules of the sII $5^{12}6^4$ large cages or 36 water molecules of the sH $5^{12}6^8$ large cages were labeled and the distances between the ether oxygen atoms (OS) and all protons (HW) of the cage waters were measured at 0.25 ps intervals along the NVE trajectory. If an OS–HW distance was less than 2.1 Å, a guest–host hydrogen bond was assumed to have formed and a "hit" was assigned to the guest at that instant. The total lifetime of each guest–host hydrogen bond was recorded and the average probability of hydrogen-bond formation in the simulation cell was determined at each temperature by averaging the ratio of times during the trajectory that all guest molecules spent hydrogen-bonded to the cage water molecules.

Acknowledgements

[1] G. A. Jeffrey in *Comprehensive Supramolecular Chemistry, Vol. 6* (Eds.: J. L. Atwood, J. E. D. Davies, D. D. MacNicol, F. Vogtle), Pergamon–Elsevier, Oxford, **1996**, pp. 757–788.

[2] a) Y. A. Dyadin, V. R. Belosludov in *Comprehensive Supramolecular Chemistry, Vol. 6* (Eds.: J. L. Atwood, J. E. D. Davies, D. D. MacNi-col, F. Vogtle), Pergamon–Elsevier, Oxford, **1996**, pp. 789–824; b) J. A. Ripmeester, C. I. Ratcliffe, K. A. Udachin in *Encyclopedia of Supramolecular Chemistry* (Eds.: J. L. Atwood, J. W. Steed), Marcel Dekker, New York, **2004**, pp. 274–280.

[3] a) A. V. Milkov, G. E. Claypool, Y.-J. Lee, W. Xu, G. R. Dickens, W. S. Borowski, *Geology* **2003**, *31*, 833–836; b) J. B. Klauda, S. I. Sandler, *Energy Fuels* **2005**, *19*, 459–470; c) S. I. MacDonald, *Annu. Rev. Energy* **1990**, *15*, 53–83; d) T. Sowers, *Science* **2006**, *311*, 838–840; e) S. G. Hatzikiriakos, P. Englezos, *Chem. Eng. Sci.* **1993**, *48*, 3963–3969; f) M. A. Maslin, E. Thomas, *Quat. Sci. Rev.* **2003**, *22*, 1729–1736; g) W. S. Reeburgh, *Chem. Rev.* **2007**, *107*, 486–513.

[4] E. D. Sloan, C. A. Koh, *Clathrate Hydrates of Natural Gases*, 3rd ed., CRC Press, New York, **2008**.

[5] H. Davy, *Philos. Trans. R. Soc. London* **1811**, *101*, 1.

[6] J. H. van der Waals, J. C. Platteeuw, *Adv. Chem. Phys.* **1958**, *2*, 1–58.

[7] a) D. W. Davidson in *Water: A Comprehensive Treatise, Vol. 2* (Ed.: F. Franks), Plenum Press, New York, **1974**; b) D. W. Davidson, Y. P. Handa, J. A. Ripmeester, J. S. Tse, J. R. Dahn, F. Lee, L. D. Calvert, *Mol. Cryst. Liq. Cryst.* **1986**, *141*, 141; c) J. A. Ripmeester, D. W. Davidson, *Mol. Cryst. Liq. Cryst.* **1997**, *43*, l09; d) J. A. Ripmeester, C. I. Ratcliffe, *J. Phys. Chem.* **1990**, *94*, 8773; e) D. H. Brouwer, E. B. Brouwer, G. MacLaurin, M. Lee, D. Parks, J. A. Ripmeester, *Supramol. Chem.* **1997**, *8*, 361–367.

[8] a) D. W. Davidson, S. R. Gough, J. A. Ripmeester, H. Nakayama, *Can. J. Chem.* **1981**, *59*, 2587; b) H. Nakayama, D. H. Brouwer, Y. P. Handa, D. D. Klug, J. S. Tse, C. I. Ratcliffe, X. Zhu, J. A. Ripmeester, *J. Am. Chem. Soc.* **1997**, *42*, 516–521.

[9] a) K. Yasuda, S. Takeya, M. Sakashita, H. Yamawaki, R. Ohmura, *J. Phys. Chem. C* **2009**, *113*, 12598–12601; b) R. Anderson, A. Chapoy, H. Haghighi, B. Tohidi, *J. Phys. Chem. C* **2009**, *113*, 12602–12607.

[10] a) T. S. Yun, J. C. Santamarina, C. Ruppel, *J. Geophys. Res. B* **2007**, *112*, B4106; b) J. Kliner, J. Grozic, *Can. Geotech. J.* **2006**, *43*, 551.

[11] a) W. R. Parrish, J. M. Prausnitz, *Ind. Eng. Chem. Process Des. Dev.* **1972**, *11*, 26–35; b) F. E. Anderson, J. M. Prausnitz, *AIChE J.* **1986**, *32*, 1321–1333; c) S. R. Zele, S.-Y. Lee, G. D. Holder, *J. Phys. Chem. B* **1999**, *103*, 10250–10257; d) A. L. Ballard, E. D. Sloan, Jr, *Fluid Phase Equilib.* **2002**, *194–197*, 371–383.

[12] D. W. Davidson, J. A. Ripmeester in *Inclusion Compounds, Vol. 3* (Eds.: J. L. Atwood, J. E. Davies, D. D. MacNicol), Academic Press, New York, **1984**, 69.

[13] a) S. Alavi, R. Susilo, J. A. Ripmeester, *J. Chem. Phys.* **2009**, *130*, 174501; b) R. Susilo, S. Alavi, I. L. Moudrakovski, P. Englezos, J. A. Ripmeester, *ChemPhysChem* **2009**, *10*, 824.

[14] a) L. J. Florusse, C. J. Peters, J. Schoonman, K. C. Hester, C. A. Koh, S. F. Dec, K. N. Marsh, E. D. Sloan, Jr., *Science* **2004**, *306*, 469; b) H. Lee, J.-W. Lee, D. Y. Kim, J. Park, Y.-T. Seo, H. Zeng, I. L. Moudra-kovski, C. I. Ratcliffe, J. A. Ripmeester, *Nature* **2005**, *434*, 743; c) D.-Y. Kim, J.-W. Lee, Y.-.T. Seo, J. A. Ripmeester, H. Lee, *Angew. Chem.* **2005**, *117*, 7927–7930; *Angew. Chem. Int. Ed.* **2005**, *44*, 7749–7752; d) Y. Park, M. Cha, W. Shin, H. Lee, J. A. Ripmeester, *J. Phys. Chem. B* **2008**, *112*, 8443–8446; e) Y. Park, M. Cha, W. Shin, J.-H. Cha, H. Lee, J. A. Ripmeester, *Proceedings of the 6th International Conference on Gas Hydrates*, ICGH: Vancouver, **2008**.

[15] SADABS Version 2.03, G. M. Sheldrick, University of Göttingen, Göttingen, **2002**.

[16] SHELXTL, Version 6.10, G. M. Sheldrick, Bruker AXS Inc., Madison, **2000**.

[17] T. C. Mak, R. K. McMullan, *J. Chem. Phys.* **1965**, *42*, 2732.

[18] K. A. Udachin, C. I. Ratcliffe, G. D. Enright, J. A. Ripmeester, *Supramol. Chem.* **1997**, *8*, 2732.

[19] H. J. C. Berendsen, J. R. Grigera, T. P. Straatsma, *J. Phys. Chem.* **1987**, *91*, 6269.

[20] W. D. Cornell, P. Cieplak, C. L. Bayly, I. R. Gould, K. M. Merz, Jr., D. M. Ferguson, D. C. Spellmeyer, T. Fox, J. W. Caldwell, P. A. Koll-man, *J. Am. Chem. Soc.* **1995**, *117*, 5179. See also, http://amber.scripps.edu.

[21] C. M. Breneman, K. B. Wiberg, *J. Comput. Chem.* **1990**, *11*, 361.

[22] DL POLY 2.16, T. R. Forester, W. Smith, CCLRC, Daresbury Laboratory, Daresbury, **2006**.

[23] a) S. Nosé, *J. Chem. Phys.* **1984**, *81*, 511; b) W. G. Hoover, *Phys. Rev. A* **1985**, *31*, 1695; c) S. Melchionna, G. Ciccotti, B. L. Holian, *Mol. Phys.* **1993**, *78*, 533.

[24] a) D. Frenkel, B. Smit, *Understanding Molecular Simulation*, 2nd ed., Academic Press, San Diego, **2000**; b) M. P. Allen, D. J. Tildesley, *Computer Simulation of Liquids*, Oxford Science Publications, Oxford, **1987**.

[25] R. K. McMullan, G. A. Jeffrey, T. H. Jordan, *J. Chem. Phys.* **1967**, *47*, 1229.

[26] G. A. Jeffrey in *Inclusion Compounds, Vol. 1* (Eds.: J. L. Atwood, J. E. Davies, D. D. MacNicol), Academic Press, New York, **1984**, pp. 135–199.

[27] P. S. R. Prasad, T. Sugahara, A. K. Sum, E. D. Sloan, Jr., C. A. Koh, *J. Phys. Chem. A* **2009**, *113*, 6540.

[28] D. Y. Kim, J. Lee, Yu.-T. Seo, J. A. Ripmeester, H. Lee, *Angew. Chem.* **2005**, *117*, 7927–7930; *Angew. Chem. Int. Ed.* **2005**, *44*, 7749–7752.

[29] D. Y. Kim, Y. Park, H. Lee, *Catal. Today* **2007**, *120*, 257–261.

[30] A. Dos, V. Schimming, S. Tosoni, H.-H. Limbach, *J. Phys. Chem. B* **2008**, *112*, 15604–15615.

[31] N. Bjerrum, *Science* **1952**, *115*, 385.